DESIGN AND EVALUATION OF A MAGNETOELASTIC TENSILE FORCE SENSOR

Šimon GANS, Ján MOLNÁR
Department of Theoretical and Industrial Electrical Engineering, Faculty of Electrical Engineering and Informatics, Technical University of Košice, Letná 9, 042 00 Košice, Slovak Republic, Tel. +421 55 602 2706, +421 55 602 2592
E-mail: simon.gans@tuke.sk, jan.molnar@tuke.sk

ABSTRACT

This paper introduces the basic theory behind magnetoelastic sensors which are based on the change of magnetic properties (permeability) due to mechanical stress (Villari effect). A well-known magnetoelastic sensor, the Pressductor, is described. A simulation model of a sensor is created, described, and evaluated by computing the static transfer characteristic of RMS secondary coil voltage change due to tensile stress. A real sensor is then manufactured from a polycrystalline transformer sheet and experimentally tested by using a tensile load created by water weight. The simulation and experiment show similar behavior but are not completely identical which is most likely since some material properties were taken from literature rather than from experimental measurements, like the magnetostriction coefficient and initial magnetic susceptibility.

Keywords: *force sensing, magnetoelastic sensor, magnetostriction, tensile stress, Villari effect*

1. INTRODUCTION

Sensors are an essential part of modern society in that they enable the automation of production processes, and they are maintaining vital parts of the industry without the need for human intervention. A parameter that determines the suitability of a sensor is its accuracy, repeatability, and other crucial statistical characteristics. The engineer who develops the specific sensor system must consider the errors, uncertainties, linearity, etc. of a given sensor to decide if the sensor fulfills the requirements. With commercial sensors, these values can be found in the specific sensor's datasheet. If such an option is not available, the values need to be evaluated experimentally.

The magnetoelastic effect is exploited in various sensor systems. It has been used for the measurement of forces acting on bodies via a bending action[2], tensile action[3], and torsional and compressive action[4]. They have been successfully used in bridge monitoring, where they continuously measure critical components under load, like cables[5] and stresses in walls of civil buildings[6]. Magnetoelastic sensors are also known for their use in cold rolling mills[7]. In the next chapters, the construction, simulation, and measurement of a magnetoelastic tensile force sensor will be described.

2. INTRODUCTION TO THE MAGNETOELASTIC EFFECT

One physical effect observed in ferromagnetic materials is the effect of magnetostriction. The effect has been first observed and documented by James Joule in 1842. By using a system of levers that were attached to an iron rod, he measured a change in its length, when the rod was magnetized. The change of dimension was small and not linear with respect to magnetic field strength. The change of a dimension relative to the demagnetized state is called the coefficient of magnetostriction (λ).

Tension, just like magnetostriction, creates internal strain in the material. At this point, it is good to mention that physical ferromagnetic effects usually do not manifest themselves alone. The ΔE effect (E – Young's modulus) also affects the strain created by magnetostriction[1].

Magnetostriction is observed in nearly all ferromagnetic materials, and it tends to be anisotropic. However, in polycrystalline materials, it is usually assumed that it is isotropic and the saturation magnetostriction is then defined by equation (1),

$$\lambda_s = \frac{2}{5} \cdot \lambda_{100} + \frac{3}{5} \cdot \lambda_{111} \tag{1}$$

in which λ_{100} and λ_{111} are the saturation magnetostriction coefficients in the crystallographic direction of a single cubic crystal. For other structures, the expressions can be found in the literature[1][8].

A simplified explanation of why magnetostriction occurs is shown below (Fig. **1**). Without the presence of a magnetic field, the magnetic domains are randomly oriented, and the net magnetization is therefore 0. When a field is applied, then all magnetic moments experience a torque that orients them parallel to the field direction. These orientation changes in turn will change the macroscopic dimensions of the sample in the field direction[9].

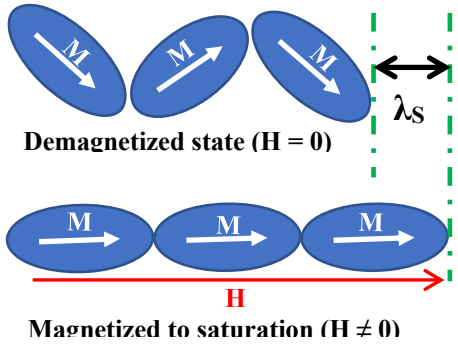

Fig. 1 Simplified explanation of the mechanism that gives rise to magnetostriction

Magnetoelasticity is directly linked to magnetostriction, and it was discovered by Emilio Villari in 1865. It is defined by the thermodynamic relation (2),

$$\frac{1}{l}\cdot\left(\frac{\mathrm{d}l}{\mathrm{d}H}\right)_{\sigma}=\left(\frac{\mathrm{d}l}{\mathrm{d}\sigma}\right)_{H} \quad (2)$$

where l is the sample dimension in the demagnetized state, H is the magnetic field intensity and σ is the mechanical stress acting on the sample[1].

The equation states that when the magnetization of the sample lengthens due to magnetostrictive strain, then external forces which change the dimensions of the sample just as much will change the magnetization accordingly[1][8].

3. ENERGY EQUILIBRIUM OF FERROMAGNETIC MATERIALS

The state of ferromagnetic materials is defined by the minimization of free energy. The total free energy of a ferromagnetic material is the sum of sub-energies, namely the:

- Exchange interaction energy
- Crystal anisotropy energy
- Magnetostriction energy
- Magnetoelastic energy
- Magnetostatic energy
- Demagnetization field energy
- Shape anisotropy energy
- Domain wall energy[8]

The total energy E_{sum} is then phrased as a variation problem denoted by equation (3), which is not possible to solve analytically. The problem can be simplified by ignoring some energy terms. The remaining energies and the relationships between them can yield useful information about the problem[8].

$$\delta E_{sum}=0 \quad (3)$$

A solution to a simplified problem, where only the magnetoelastic and total magnetic energy were considered was shown in [10]. The resulting equation (4) expresses the change of permeability due to external stresses, where B_S is the magnetic flux density at saturation, λ_{ms} is the magnetostriction coefficient at saturation and μ is the permeability of the unstressed material[10].

$$\Delta\mu=\frac{2\cdot\lambda_{ms}}{B_S^2}\cdot\mu^2\cdot\sigma \quad (4)$$

In praxis, evaluating sensor performance is mostly done via simulation programs like COMSOL Multiphysics. Because the inductance of an iron core inductor is directly proportional to the permeability of the core material, the changes that arise from stressing it can be measured electrically as a coil impedance change or coupling factor change in transformer-like sensors.

4. PRESSDUCTOR TYPE SENSOR

A well-known design of magnetoelastic sensors is the "Pressductor", which is shown below (Fig. **2**). It is usually manufactured into a square shape with 4 holes, in which the magnetizing and sensing coils are placed. It is constructed by stacking many electrically isolated layers of thin ferromagnetic sheets together to suppress eddy currents. Continuous development of advanced materials like amorphous metals has enabled the improvement of the linearity and other characteristics of such sensors[11].

The operating principle is based on the change of permeability in the direction of applied force as shown in (4). The magnetizing and sensing coils are perpendicular to each other, so when assuming perfect material isotropy, no voltage is induced in the sensing coil. Because the sheet is thin, the thickness dimension can be ignored and a 2D analysis can be used. The magnetizing coil creates a magnetic field of intensity H, which creates a magnetic flux density B inside of the material described in (5)[11].

$$B=\mu\cdot H \quad (5)$$

The permeability of a 2D material is expressed by a permeability tensor with components shown in (6)[11].

$$\mu=\begin{vmatrix}\mu_x & 0\\ 0 & \mu_y\end{vmatrix} \quad (6)$$

By using the square sides as the cartesian coordinate system axes x and y, the permeabilities μ_x and μ_y determine magnetic flux densities B_x and B_y respectively. Because the sensing coil is at a 45° angle to the coordinate system axes, the flux intersecting the sensing coil is defined by (7),

$$B_S=-\frac{\sqrt{2}}{2}\cdot B_x+\frac{\sqrt{2}}{2}\cdot B_y \quad (7)$$

where B_S is the flux component in the direction of the sensing coil axis[11].

In the unstressed state B_x and B_y are equal, so B_S and therefore the induced voltage will be equal to 0. The induced voltage in a coil is defined by equation (8),

$$u(t)=-n\cdot S\cdot\frac{\mathrm{d}B_S}{\mathrm{d}t} \quad (8)$$

In which u is the induced voltage, S is the area coil area and n is the number of coil turns. When mechanical stress in one direction changes equality between the tensor components, then B_S will no longer be zero and voltage will be induced[11].

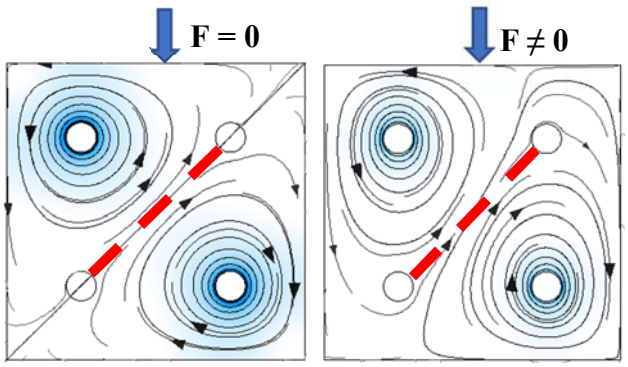

Fig. 2 Pressductor sensor shape. When no force is applied, no magnetic field lines (red closed curves) intersect the diagonal coil. If a force is present, the stress-induced anisotropy changes the flux path, which then intersects the sensing coil (the red dashed line)

5. MAGNETOELASTIC SENSOR DESIGN

A "Pressductor" sensor was designed, based on the principle analyzed in the previous chapter. A technical model was drawn in Fusion 360 and is shown below (Fig. 3).

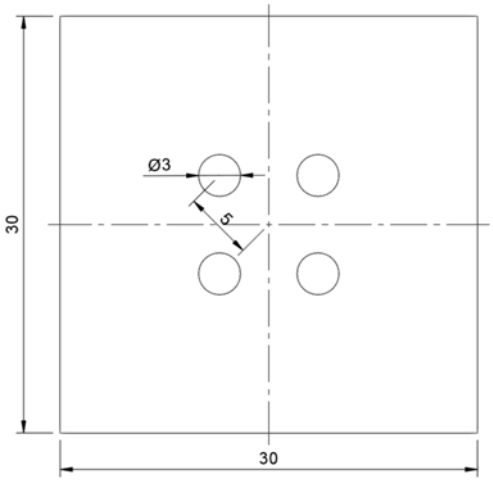

Fig. 3 Dimensions of the designed pressductor sensor in millimeters

Fig. 4 3D model of the pressductor with the magnetizing and sensing coils. The coils are modeled as one single, homogenous turn of wire

A 2D analysis was done to estimate the sensor's response to applied tensile forces utilizing finite element analysis. The COMSOL Multiphysics software was used with coupled magnetic and structural mechanics modules. The magnetostrictive behavior of the material was defined to be nonlinear and isotropic[12]. Magnetic hysteresis modeling was omitted to reduce computation times, so an anhysteretic magnetization curve model was used, described by the Langevin function. The force applied varied from 0 to 10 N in 1 N steps and was applied homogenously on one of the sensor's square sides. The maximum mechanical stress exerted on the sensor is defined by (9),

$$\sigma = \frac{F}{A} = \frac{F}{d \cdot l} = \frac{10}{0.0005 \cdot 0.03} \doteq 6,\bar{6} \cdot 10^5\ Pa \tag{9}$$

where F is the force, A is the area on which the force is applied, d is the thickness of the sheet and l is the length of the sheet's side.

The 2D geometry was imported into COMSOL Multiphysics from Fusion 360 via a DXF file and is shown below (Fig. 5).

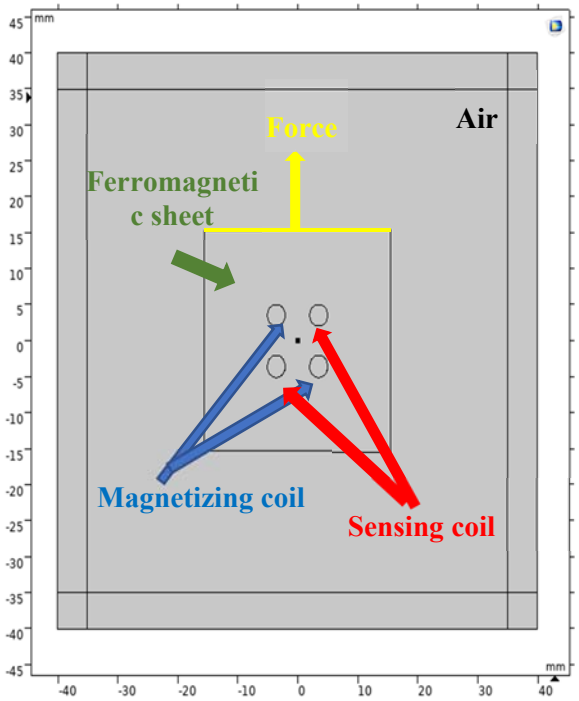

Fig. 5 The imported 2D geometry of the system. The sensor is placed inside an air domain. The coils have been given copper material properties

One 0.3 mm thick anisotropic polycrystalline transformer steel sheet was used for the sensor material. The cut square had the same position and dimensions of holes as shown in Fig. 3. Each coil consists of 15 turns of copper wire with a diameter of 0.3 mm.

The magnetizing current into the sensor was supplied by a regulated sinusoidal voltage source (AC250K1D-S) with a step-down transformer with a coil ratio of 10:1 connected to its output to increase the resolution of the output voltage amplitude 10-fold in the 0 – 2 V range. A sinusoidal voltage signal with a frequency of 50 Hz with an amplitude of 0.3 V was connected to the magnetizing winding which created a sinusoidal-like current with an amplitude of 1.5 A, which was also used in the simulation. The simulation results are shown below (Fig. 6). The data was further analyzed, and a graph of RMS voltage changes due to stress relative to the unstressed state was drawn (Fig. 7). At the largest simulated stress ($6{,}6 \cdot 10^5$ Pa), the voltage amplitude across the sensing coil reached approximately 51 µV which translates to an RMS voltage change of 36 µV compared to the unloaded state. The sensing coil was connected to a differential op-amp amplifier to amplify the voltage to more easily measurable levels. The block diagram of the system can be seen in the figure (Fig. 8) and is described in the next chapter.

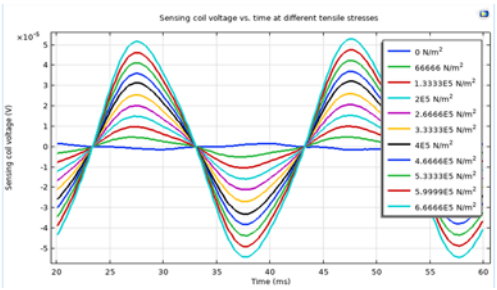

Fig. 6 The simulated sensing coil voltage changes at different tensile stresses

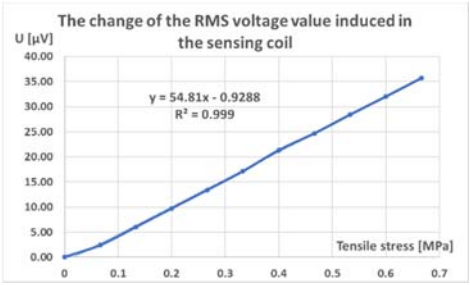

Fig. 7 Graph of voltage changes due to tensile stress with shown linear interpolation function of the data

The magnetic material characteristics of the transformer sheet have been taken from the literature [13] and are characteristics of similar types of materials (saturation magnetization M_S = 1.5.10^6 A/m, initial susceptibility χ_i = 2500). Measuring these characteristics directly for the sheet material will be done in future work.

6. EXPERIMENTAL SETUP

The figure (Fig. 8) shows the diagram of the voltage amplifier. The output of the amplifier is connected to an oscilloscope. The input current and output voltage were measured on an oscilloscope and the measurements are shown below (Fig. 12 and Fig. 13).

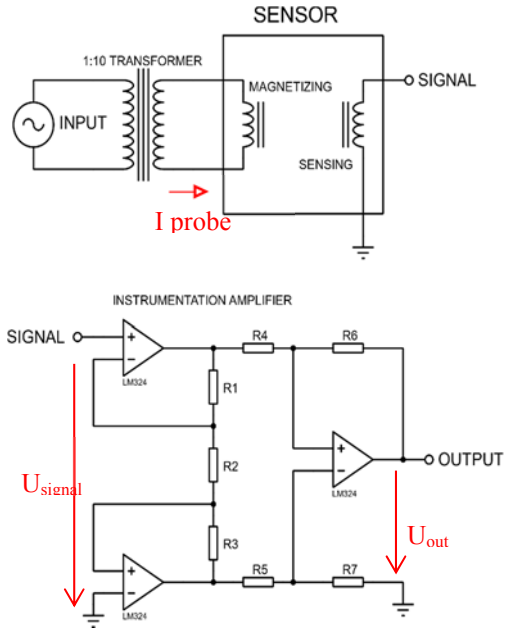

Fig. 8 Schematic of the amplifier. The electrical quantities marked by red color were measured on an oscilloscope

The amplifier stage consists of 3 LM324 operational amplifiers connected as a high input impedance differential instrumentation amplifier. The voltage gain is expressed by equation (10) if $R_1 = R_3$, $R_4 = R_5$, and $R_6 = R_7$[14].

$$A_{voltage} = \left(1 + \frac{2 \cdot R_1}{R_2}\right) \cdot \frac{R_6}{R_4} \tag{10}$$

Resistor values $R_2 = R_4 = R_5$ = 100 kΩ and $R_1 = R_3 = R_6 = R_7$ = 680 kΩ, determined the voltage gain to a value of 98.4. Because one end of the sensor coil is grounded a single inverting or non-inverting opamp amplifier configuration could have been used, but because the circuit was set up on a breadboard, parasitic capacitances, and parasitic induced voltages were present between the ground of the circuit and the grounded end of the secondary coil. Therefore a configuration with a high common-mode rejection ratio was used as it is in the case of the instrumentation amplifier. Using a simple differential amplifier was quite noisy and a lot more stable results were obtained with the instrumentation amplifier. A fully integrated instrumentation op-amp into one package could be used as well (like the low noise INA849 from Texas Instruments), but discrete opamps were used because at the time they were available at the laboratory and were fulfilling the task well.

The sensor itself is depicted in the picture below (Fig. 9). Wooden slats were glued to the opposite ends of the pressductor on which tensile force was applied.

Fig. 9 Pressductor sensor sheet with the magnetizing and sensing winding

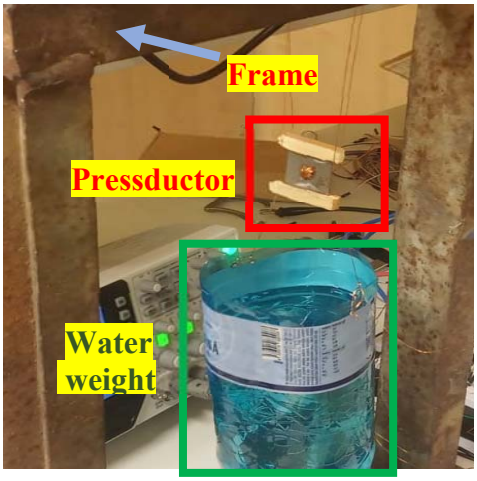

Fig. 10 Setup of loading the pressductor sensor with water weight

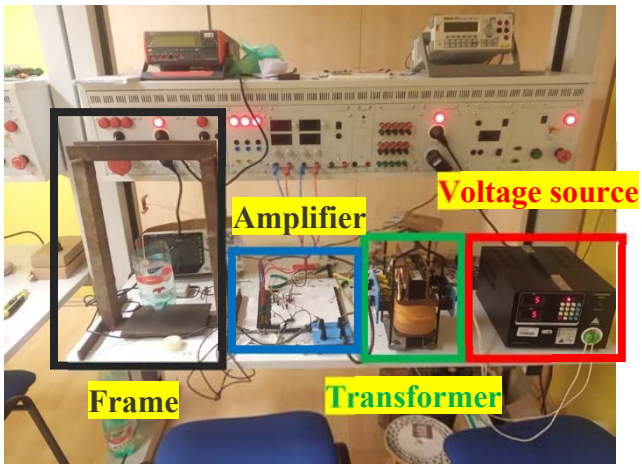

Fig. 11 The input source of the pressductor. The output amplifier was connected on a breadboard

The pressductor was secured to a metal frame with copper wire. A water container was secured to the opposite side of the Pressductor. Equal volume amounts of water (approx.. 88 milliliters) were added to the container. Since the water density at 20 °C in standard atmospheric pressure is 998,29 kg/m^3, the tensile force acting on the sensor is equal to the gravitational force by which the water is pulled downwards to the ground, which is expressed by (11), where F is the force, V is the volume, ρ_{H20} is the density of water and g is the gravitational acceleration (approx. 9,81 m.s^{-2}). The force created by the container itself is considered as the unstressed state.

$$F = V \cdot \rho_{H2O} \cdot g \tag{11}$$

The unamplified output voltage and input current waveform of the sensor at zero force is shown below (Fig. 12). The current amplitude was 1,1 A and the voltage peaks reached an amplitude of 13 mV.

Fig. 12 The output voltage (blue) and input current (yellow) waveforms of the sensor

After voltage amplification, the unstressed voltage waveform reached peaks of 1.14 V at zero force. The amplification did not change the waveform shape, which can be seen below (Fig. 13). The LM324 operational amplifiers were supplied by ± 10 V.

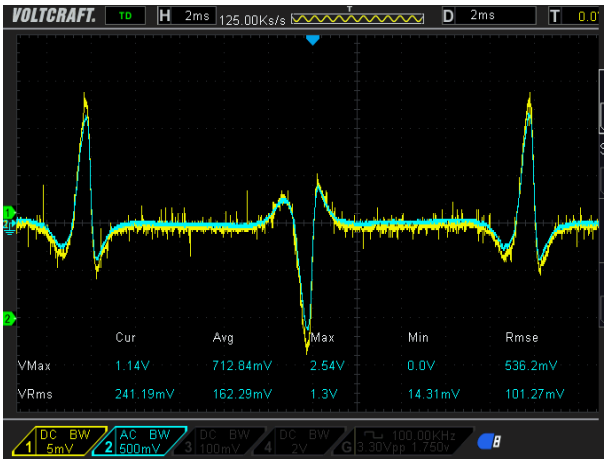

Fig. 13 The unamplified output voltage (yellow) and amplified output voltage (blue). The waveforms overlap because the oscilloscope ranges ratio was 100 - the same as the voltage gain

At zero force the output should be zero, but due to construction flaws, the windings are not perfectly perpendicular to each other and small angle deviations between individual coil turns in addition to capacitive coupling between the coils are probably the reason behind the nonzero voltage at zero force combined with capacitive coupling between the windings and the fact that the transformer sheet material is anisotropic.

7. RESULTS

Changes in the secondary coil RMS voltage were measured (which was computed on the oscilloscope in real-time). The measurement was done when the force was increasing from no load to full load and when it was decreasing from full load to no load. This was done to determine the maximum hysteresis error, which is usually large in the case of magnetoelastic sensors compared to other types of force-sensing devices. The RMS value was computed as an average of multiple periods and the static transfer characteristic can be seen below (Fig. 14). The measurement at increasing and decreasing force is shown in Fig. 15. In Fig. 13 the voltage amplitude reaches values of 1,14 V, which corresponded to an RMS voltage of 241,19 mV. With increasing force the output RMS voltage changes just by a few mV compared to the unstressed state which is shown in the graph below.

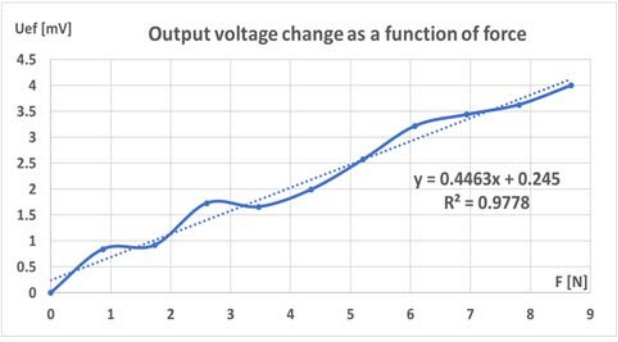

Fig. 14 Output characteristic of the sensor. The force increased with time. The maximum linearity error was 0,322 N or approximately 3,72 %

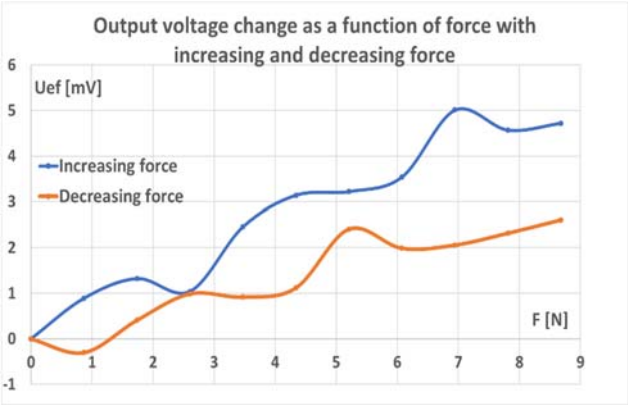

Fig. 15 Output characteristic of the sensor. The force first decreased and then increased to estimate the hysteresis error. The largest absolute hysteresis measured was 2,95 mV or approximately 33,99 % of hysteresis error

Previous works like [11] showed that the hysteresis error is strongly dependent on the input signal characteristics. A 33,99 % hysteresis error is rather large, while the 3,72 % linearity error is more acceptable for example for a rough estimation of the applied, but it is still not satisfactory for commercial use. Simulation results also showed that the position of the holes for the windings also affects the sensitivity of the sensor. Experimentally proving it will be the subject of future work. Further experimentation with different input power characteristics (frequencies, amplitudes, waveforms) is in progress. The comparison between the simulated and experimental results is shown below (Fig. 16).

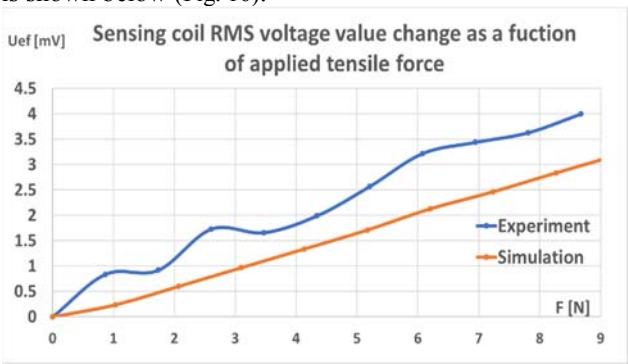

Fig. 16 Comparison between the simulated and experimental results of the force sensor

The curves have a similar slope, but the experimental curve shows a higher stress sensitivity which could be explained by capacitive coupling between the windings and the construction flaws, which were already mentioned.

8. CONCLUSIONS

The paper presented a brief overview of the magnetoelastic effect and the principle of operation of a well-known magnetoelastic force sensor - the "pressductor". The simulation and experimental results were compared with each other. Magnetic material properties are known to show large variations even if they are measured in different places of the same steel sheet[13]. This means that to accurately model sensors of this type, the magnetic properties should be measured for the given samples and imported into the simulation. Assuming isotropy of material characteristics can be another source of error because magnetic properties of materials that are considered isotropic usually vary up to several percent in different directions. Including a model which incorporates hysteresis like by using the Jiles-Atherton model of ferromagnetic hysteresis can also lessen the gap between experimental and simulation results[15]. Also defining the anhysteretic magnetization by using the Langevin function in the case of some materials might not be sufficiently accurate and other magnetization models are available that define the function between *H* and *M* better.

9. FUTURE WORK

The main mentioned causes of differences between the simulation model and the real sensor will be addressed. The constant voltage source will be replaced by a constant current source, where the output amplitude and frequency can be varied. Multiple sensors have been made and are being measured to find the most optimal hole configuration. An automated measurement system will be established to make the measurement process less time-consuming.

ACKNOWLEDGMENTS

The authors thank for the financial support from the GRANT FEI 2022 project for the grant specified by the index FEI-2022-82 which helped in the research.

REFERENCES

[1] LEE, E. W.: Magnetostriction and Magnetomechanical Effects, 1955, Rep. Prog. Phys. 18 184, IOP Publishing. Available on the internet: Magnetostriction and Magnetomechanical Effects - IOPscience.

[2] GRENDA, P. – KUTYŁA, M. – NOWICKI, M. – CHARUBIN, T.: Bendductor – Transformer Steel Magnetomechanical Force Sensor, MDPI Sensors 2021, 21(24), 8250. DOI: 10.3390/s21248250. Available on the internet at: https://www.mdpi.com/1424-8220/21/24/8250?type=check_update&version=1

[3] NOWICKI, M.: Tensductor – Amorphous Alloy Based Magnetoelastic Tensile Force Senso, 2018, 18(12), 4420. DOI : 10.3390/s18124420. Available on the internet at: https://www.mdpi.com/1424-8220/18/12/4420

[4] BIÉNKOWSKI, A. – SZEWCZYK, R. – SALACH, J.: Indutrial Application of Magnetoelastic Force and Torque Senors, Acta Physica Polonica A, 2010, Vol. 118, No. 5. DOI: 10.12693/APhysPolA.118.1008. Available on the internet at: https://www.researchgate.net/publication/287486587_Industrial_Application_of_Magnetoelastic_Force_and_Torque_Sensors

[5] WANG, M. L. – SATPATHI, D. – KOONTZ, S. – JAROSEVIC, A. – CHANDOGA, M.: Monitoring of cable forces using magneto-elastic sensors, 1999, Computational Mechanics in Structural Engineering,

pages 337-347. DOI: 10.1016/B978-008043008-9/50064-8. Available on the internet at: https://www.sciencedirect.com/science/article/pii/B9780080430089500648

[6] AUASNIO, G. – BARONE, A. C. – HISON, C. – MANNARA, G. – LANOTTE, L.: Magnetoelastic sensor application in civil buildings monitoring, 2005, Elsevier Senor and Actuators A, 123-124, Pages 290-295. DOI: 10.1016/j.sna.2005.03.027. Available on the internet: https://www.sciencedirect.com/science/article/pii/S0924424705001652

[7] DAHLE, O.: The pressductor and the torductor – two heavy-duty transducers based on magnetic stress sensitivity, 1964, IEEE Transactions on Communication and Electronics, vol. 83, issue 75, pages 752-758. DOI: 10.1109/TCOME.1964.6592601. Available on the internet at: https://ieeexplore.ieee.org/abstract/document/6592601/authors#authors

[8] HAJKO, V. – POTOCKÝ, L.: Fyzika magnetických látok, 1973, UPJŠ, ES-UPJŠ 10/64/73, pages 252-306

[9] BIÉNKOWSKI, A. – SZEWCZYK, R.: Magnetostrictive Properties of MnO.70ZnO.24Fe2.06O4 Ferrite, MDPI materials, 2018, 11(10), 1894. Available on the internet at: https://www.mdpi.com/1996-1944/11/10/1894?type=check_update&version=1

[10] TOMČÍKOVÁ, I.: Modeling of magnetic field distribution in magnetoelastic force sensor, 2018, ResearchGate, DOI: 10.30929/2072-2058.2018.1.41.38-45. Available on the internet at: https://www.researchgate.net/publication/266292425_MODELING_OF_MAGNETIC_FIELD_DISTRIBUTION_IN_MAGNETOELASTIC_FORCE_SENSOR

[11] NOWICKI, M.: Tensuctor – Amorphous Alloy Based Magnetoelastic Tensile Force Sensor, 2018, 18(12), 4420, MDPI sensors. Available on the internet at: https://www.mdpi.com/1424-8220/18/12/4420

[12] COMSOL Multiphysics 6.0 documentation, Nonlinear Magnetostrictive Transducer. Available on the internet at: https://www.comsol.com/model/download/964581/models.sme.nonlinear_magnetostriction.pdf

[13] REINBOTH, H.: Vlastnosti a použití magnetických materiálu, Praha 1975, DT 621.318.1/.13

[14] ElectronicsTutorials, The Differential Amplifier. Available on the internet at: https://www.electronics-tutorials.ws/opamp/opamp_5.html

[15] GANS, Š. – MOLNÁR, J.: The Jiles-Atherton Model of ferromagnetic materials and its dependence on the anhysteretic magnetization, JIEE, ISSN 2454-0900, 2021. Available on the internet at: http://www.jiee.eu/the-jiles-atherton-model-of-ferromagnetic-materials-and-its-dependence-on-the-anhysteretic-magnetization/

Received March 3, 2023, accepted March 23, 2023

BIOGRAPHIES

Šimon Gans was born in 1997. In 2021 he graduated (Master's degree) with distinction from the department of Theoretical and Industrial Electrical Engineering of the Faculty of Electrical Engineering and Informatics at Technical University in Košice. Since 2021 he is working as a Ph.D. student in the same department, where he is teaching electrical engineering and circuit theory. His scientific research is focusing on the optimization and simulation of magnetoelastic sensors.

Ján Molnár is an associated professor at the Department of Theoretical and Industrial Electrical Engineering at the Technical University of Košice. He has been working in this position at the Department since 2017. He was awarded his doctoral degree (PhD.) at the Department of Theoretical Electrical Engineering and Electrical Measurement at the Technical University of Košice in 2011. He received his master's degree in Electrical Measurements from the Technical University of Košice in 2003. He is an author of several patents and a reviewer of several international journals. His specialization is including automated measurements and control chains, IoT, Machine-to-Machine communication, and computer systems.